AJNR

MR Imaging of Parotid Tumors: Typical Lesion Characteristics in MR Imaging Improve Discrimination between Benign and Malignant Disease

A. Christe, C. Waldherr, R. Hallett, P. Zbaeren and H. Thoeny

AJNR Am J Neuroradiol 2011, 32 (7) 1202-1207
doi: https://doi.org/10.3174/ajnr.A2520
http://www.ajnr.org/content/32/7/1202

ORIGINAL RESEARCH

MR Imaging of Parotid Tumors: Typical Lesion Characteristics in MR Imaging Improve Discrimination between Benign and Malignant Disease

A. Christe
C. Waldherr
R. Hallett
P. Zbaeren
H. Thoeny

BACKGROUND AND PURPOSE: The surgical approach to parotid tumors is different for benign and malignant neoplasms, but the clinical symptoms do not correlate well with histology. Difficulties in tumor classification also arise in imaging modalities, in which sonography has the lowest and MR imaging, the highest accuracy. The purpose of this study was to review our experience using conventional MR imaging of the neck in the evaluation of parotid tumors and to evaluate which MR imaging findings are best able to predict malignant histology.

MATERIALS AND METHODS: Eighty-four consecutive patients (43 males, 41 females; median age, 56 years; range, 9–85 years) with parotid gland tumors who underwent MR imaging before surgery were prospectively included in the present study and retrospectively analyzed. Histology was available for all tumors. We analyzed the following MR imaging parameters: signal intensity, contrast enhancement, lesion margins (well-defined versus ill-defined), lesion location (deep/superficial lobe), growth pattern (focal, multifocal, or diffuse), and extension into neighboring structures, perineural spread, and lymphadenopathy.

RESULTS: The 57 (68%) benign and 27 (32%) malignant tumors consisted of 29 pleomorphic adenomas, 17 Warthin tumors, 11 various benign tumors, 5 mucoepidermoid carcinomas, 3 adenoid cystic carcinomas, 1 acinic cell carcinoma, 1 carcinoma ex pleomorphic adenoma, 9 metastases, and 8 various malignant neoplasms. Specific signs predictive of malignancy were the following: T2 hypointensity of the parotid tumor ($P = .048$), ill-defined margins ($P = .001$), diffuse growth ($P = .012$), infiltration of subcutaneous tissue ($P = .0034$), and lymphadenopathy ($P = .012$).

CONCLUSIONS: Low signal intensity on T2-weighted images and postcontrast ill-defined margins of a parotid tumor are highly suggestive of malignancy.

ABBREVIATIONS: DWI = diffusion-weighted imaging; FNP = fine-needle puncture; ROC = receiver operating characteristic analysis; SENSE = sensitivity encoding; 1-SPEC = 1-specificity; SI = signal intensity; TIRM = turbo inversion-recovery magnitude; TSE = turbo spin-echo

Parotid tumors are uncommon neoplasms that account for approximately 3% of all head and neck tumors.[1] Local excision or superficial parotidectomy are established surgical procedures for patients with benign lesions; with malignant tumors, the patients usually undergo total parotidectomy, with potential sacrifice of the facial nerve. Clinical findings have limitations in diagnosing malignant parotid neoplasms: Only a few clinical symptoms, such as facial nerve palsy, allow the diagnosis of malignancy, and most parotid tumors grow slowly, whether benign or malignant. Therefore, preoperative imaging has assumed a major role in surgical planning for assessing the location and malignancy of the tumor. It is useful to understand typical MR imaging features of parotid tumors, which have been reported with respect to SI characteristics.[2-24] The purpose of our study was to critically assess our experience in 84 consecutive patients to detect specific imaging findings, on conventional MR imaging, predictive of malignancy. Furthermore, our study aimed to describe the distribution of lesions and the typical MR imaging appearances for various parotid tumors in our cohort.

Received July 21, 2010; accepted after revision November 20.

From the Departments of Diagnostic, Interventional and Pediatric Radiology (A.C., H.T.), and Oto-Rhino-Laryngology, Head and Neck Surgery (P.Z.), Inselspital, University Hospital, University of Bern, Bern, Switzerland; Department of Radiology (C.W.), Engeried Hospital, Bern, Switzerland; and Department of Radiology (R.H.), Stanford University School of Medicine, Stanford, California.

Please address correspondence to Andreas Christe, MD, Department of Diagnostic, Interventional and Pediatric Radiology, Inselspital, University Hospital, University of Bern, Freiburgstr 10, CH-3010 Bern, Switzerland; e-mail: andreas.christe@insel.ch

Indicates article with supplemental on-line table.

DOI 10.3174/ajnr.A2520

Materials and Methods

Patient Characteristics and Distribution of Tumors in this Cohort

Ninety-nine consecutive patients with clinical suspicion of parotid tumors underwent cross-sectional imaging at our institution between November 2004 and January 2009. Eighty-four patients underwent MR imaging; the remaining 15 patients underwent CT (MR imaging contraindication) for surgical planning. Only those 84 patients (41 females, 43 males; median age, 56 years; range, 9–85 years) who underwent MR imaging were prospectively included in the present study and retrospectively analyzed. Indications for surgery were assessed by the ear, nose, and throat surgeon of our hospital. All tumors were surgically resected and histologically classified. The local ethics committee approved the study.

MR Imaging

After exclusion of contraindications, all patients gave their written informed consent to undergo MR imaging of the neck. A 1.5T MR imaging unit (Magnetom Sonata; Siemens, Erlangen, Germany) with

a neck coil (CP Neck Array; Siemens) was used for imaging. The standard MR imaging neck protocol included 7 sequences from the base of the skull to the apex of the lung, and the examination time did not exceed 1 hour. The parameters were the following—a coronal TIRM sequence: TR, 5620 ms; TE, 28 ms; section thickness, 4 mm; distance factor, 30%; FOV, 340 mm; resolution, 512; voxel size, 1.3 × 0.7 × 4.0 mm; an axial TIRM sequence: TR, 4000 ms; TE, 20 ms; section thickness, 3 mm; distance factor, 20%; FOV, 280 mm; resolution, 512; voxel size, 1.1 × 0.5 × 3.0 mm; an axial T2-weighted TSE sequence: TR, 3930 ms; TE, 76 ms; section thickness, 3 mm; distance factor, 20%; FOV, 280 mm; resolution, 512; voxel size, 1.1 × 0.5 × 3.0 mm; an axial T1-weighted TSE sequence: TR, 687 ms; TE, 12 ms; section thickness, 3 mm; distance factor, 20%; FOV, 280 mm; resolution, 512; voxel size, 1.1 × 0.5 × 3.0 mm; an axial gadolinium-enhanced T1 TSE fat-saturated sequence; TR, 693 ms; TE, 12 ms; section thickness, 3 mm; distance factor, 20%; FOV, 280 mm; resolution, 512; voxel size, 1.1 × 0.5 × 3.0 mm; a coronal gadolinium-enhanced T1 TSE fat-saturated sequence: TR, 693 ms; TE, 12 ms; section thickness, 4 mm; distance factor, 30%; FOV, 340 mm; resolution, 512; voxel size, 1.3 × 0.7 × 4.0 mm; and a sagittal gadolinium-enhanced T1 TSE fat-saturated sequence: TR, 693 ms; TE, 12 ms; section thickness, 4 mm; distance factor, 30%; FOV, 340 mm; resolution, 512; voxel size, 1.3 × 0.7 × 4.0 mm.

Image Analysis

Two board-certified radiologists (subspecialized in head and neck radiology) evaluated the MR images on a PACS workstation (Philips Medical Systems, Best, the Netherlands) by consensus. Image findings are classified in the On-line Table.

SI on T1-weighted images was judged as low (hypointense) when the SI of the parotid tumor was equal to or lower than the SI of muscles, moderate (hyperintense) when the SI was brighter than muscle, and strong (highly hyperintense) when the SI was closer to the SI of fatty tissue than of muscle. T2-weighted and TIRM characteristics were reported as low (hypointense) when the SI of the tumor was lower than that of parotid tissue, moderate (hyperintense) when the SI was equal to or brighter than that of normal parotid tissue, and strong (highly hyperintense) when the SI was closer to that of water (CSF) than of parotid tissue. For heterogeneous lesions, the SI of the portion representing >50% of the tumor was used to classify the SI. Enhancement of the tumor was divided into low (equal or less enhancement than muscle), intermediate (more enhancement than muscle, similar to normal parotid tissue), and strong (more enhancement than parotid tissue, like vessels).

Furthermore, the tumor appearance was classified into homogeneous and heterogeneous, on both pre- and postcontrast sequences. The tumor was classified as inhomogeneous when >10% of the tumor had a different SI on T2- or T1-weighted images after intravenous contrast administration. The lesion border was classified as well-defined and ill-defined on both pre- and postcontrast imaging. When the border was blurred or ill-defined at only 1 point, the whole border was deemed ill-defined. The lesion growth pattern was graded into focal, multifocal, and diffuse (involving the entire parotid gland). Appearance was classified into polylobulated (convex outpouchings) and cystic/necrotic, with the latter defined as an area without enhancement. We assessed the following lesion locations: unilateral, bilateral, superficial lobe, parotid tail, deep lobe, or both lobes. A virtual line drawn from the lateral border of the posterior belly of the digastric muscle and the retromandibular vein to the lateral edge of the mandible was used for locating the superficial and deep lobes.[11,25] The approximate tumor volume was calculated by using the product of tumor length, width, and depth and the multiplication factor $\pi/6$.

Infiltration of surrounding tissue was classified as extension into the subcutaneous tissue, skin, masticator space, or mandible. Infiltration was confirmed by visualization of a T1 hypointense enhancing mass. Perineural spread was defined as an enhancing mass along cranial nerve V and VII. Lymphatic spread was defined as a visualized lymph node with a longitudinal diameter of >12 mm[13] and a short-axis diameter of >10 mm or with visualized necrosis. All nodal stations of the neck were searched.

Performance of Radiologists

The blinded readers stratified the tumors into malignant and benign and tried to make the histologic diagnosis in consensus on the basis of their knowledge and experience (10 and 5 years of experience in head and neck MR imaging).

Statistical Analysis

Each MR imaging finding among benign parotid tumors was compared with those in malignant tumors by the Fisher exact test, except for patient age and the volume of the tumor, which were compared by the Wilcoxon rank sum test. An MR imaging finding with a P value $< .05$ (2 SD) was considered significant. MR imaging signs with P values $\geq .05$ were rated as not significant. P values between .05 and .32 (1 SD) were considered indicative of a certain tumor. Radiologic performance was reported as the sensitivity and specificity for malignant tumors and the percentage of correct diagnoses. Furthermore, MR imaging findings of the most frequent histologic entities were compared with the rest of the tumors by the same statistical analysis, to define typical signs for each tumor. ROCs were calculated for significant numeric values like patient age and tumor volume.

Results

Patients: Distribution of Tumors

The consecutive sample of 84 clinical tumors consisted of 57 (68%) benign and 27 (32%) malignant tumors. Of the benign entities, there were 29 (34%) pleomorphic adenomas, 17 (20%) Warthin tumors, 3 (4%) granulomatous inflammations, and 8 (10%) various tumors, including 3 oncocytomas, 2 intraductal papillomas, 1 basal cell adenoma, 1 schwannoma, and 1 epidermoid cyst. The 27 malignant tumors consisted of 5 (6%) mucoepidermoid carcinomas, 3 (4%) adenoid cystic carcinomas, 1 (1%) acinic cell carcinoma, 1 (1%) carcinoma ex pleomorphic adenoma, 2 (2%) adenocarcinomas and 2 (2%) lymphomas, 1 (1%) myoepithelial carcinoma, 1 (1%) Ewing sarcoma, 1 (1%) undifferentiated carcinoma, 1 (1%) salivary duct carcinoma, and 9 metastases (11%, comprising 5 squamous cell carcinomas of the skin, 3 melanomas, 1 thyroid cancer).

MR Imaging Findings

A low SI on T2-weighted images was significantly more likely in malignant than in benign tumors ($P = .048$): Twenty-six percent of malignant cases and only 9% of benign tumors showed a hypointense mass on T2-weighted images (Fig 1, On-line Table). Conversely, a tumor that showed strong SI on T2-weighted images was likely benign ($P = .038$). The best MR imaging finding for differentiating malignant from benign tumor was an ill-defined margin after intravenous contrast ad-

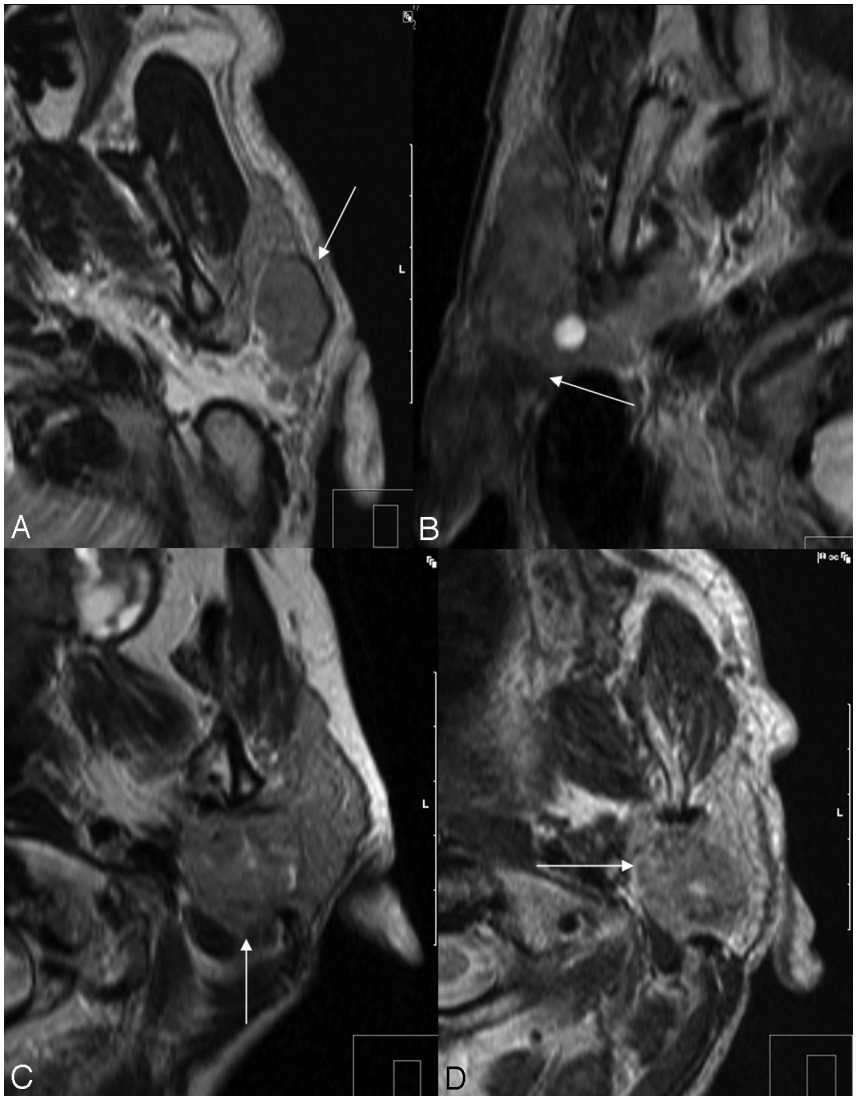

Fig 1. Low SI on axial T2-weighted images as a sign of malignancy. *A,* Non-Hodgkin lymphoma of a 44-year-old male patient. *B,* A 76-year-old man with parotid infiltration of a squamous cell carcinoma of the skin. *C,* Myoepithelial carcinoma of a 54-year-old female patient in the deep parotid lobe. *D,* Adenoid cystic carcinoma of a 54-year-old woman.

ministration (Fig 2): Fifty-nine percent of malignant tumors and only 21% of benign entities showed ill-defined borders ($P = .001$). Before contrast administration, ill-defined or blurred borders of malignant tumors were a little less obvious ($P = .016$). Malignant tumors typically showed a diffuse ($P = .012$) or multifocal ($P = .031$) growth pattern, with infiltration of the subcutaneous tissue ($P = .003$) and the masticator space ($P = .012$). Subcutaneous tissue infiltration appeared in 33% of malignant tumors and in only 7% of benign lesions. Frequently malignant tumors showed perineural spread ($P = .003$, Fig 3), and lymphadenopathy ($P = .012$) occurred in 22% of malignant lesions versus only 4% of benign tumors. Benign tumors had a predilection for the superficial parotid lobe ($P = .005$), with malignant lesions tending to arise in the deep lobe or in both lobes ($P = .081$ or $.048$).

The tumor volume and patient age did not significantly correlate with benignity, though there was a tendency for benign tumors to appear at an earlier age ($P = .069$). The median age of patients with benign tumors was 55 years (mean, 51 years; range, 14–81 years) compared with 61 years for malignant tumors (mean, 57 years; range, 9–85 years). The ROC predicted the highest accuracy for detection of malignancy at a cutoff age of older than 47 years but still only reached a sensitivity of 78% with a specificity of 44%. There was no sex preference in benign or malignant tumors.

Cystic/necrotic areas did not help distinguish malignant from benign tumors, being present in even more benign (54%) than malignant tumors (41%, $P = .35$). The highest accuracies for prediction of malignant tumors were found for perineural spread and subcutaneous tissue infiltration (both 74%, On-line Table), followed by ill-defined borders after contrast administration (73%), and low SI on T2-weighted images (70%). While the first 2 mentioned MR imaging findings had low sensitivities (19% and 33%, respectively) compared with high specificities (100% and 93%, respectively), the feature "ill-defined border postcontrast" reached a sensitivity of 59% with a specificity of 79%.

Performance of Radiologists

In prediction of malignancy, the 2 readers reached a sensitivity of 67% and a specificity of 81% in consensus reading (On-line Table). A large difference was found in the correctness of the

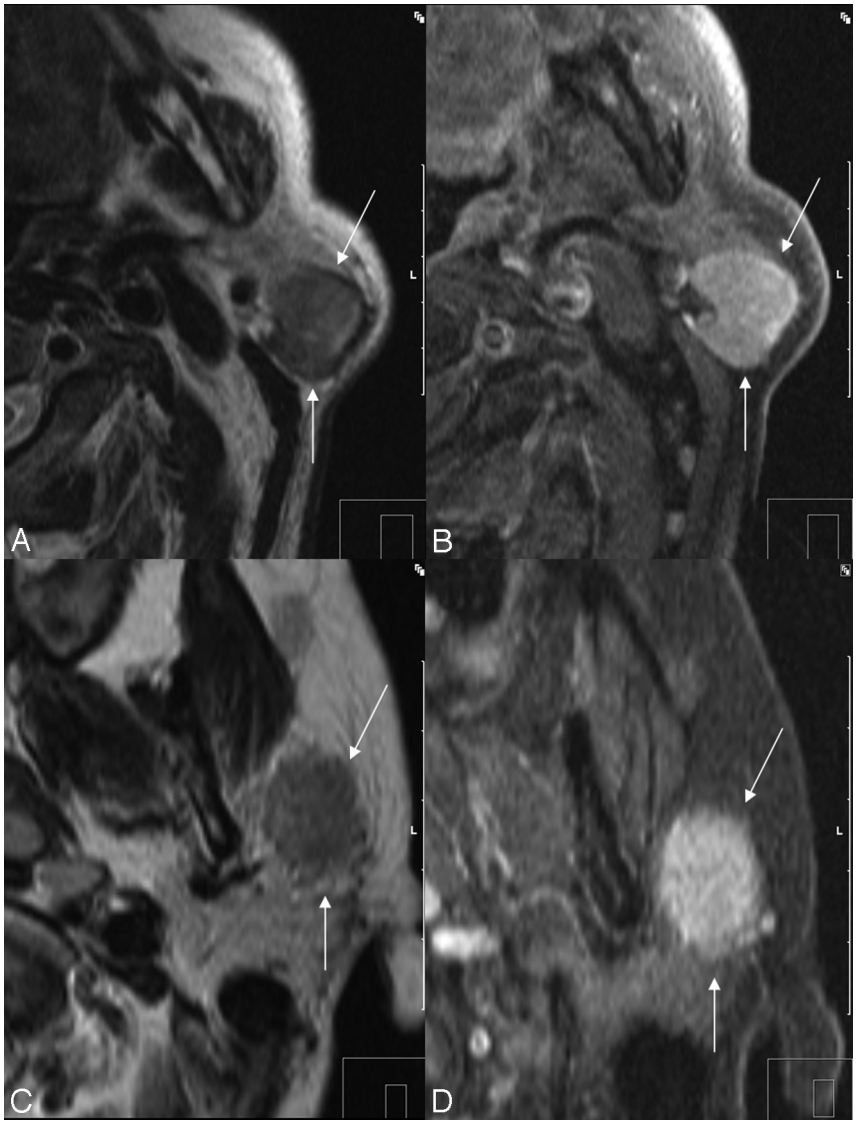

Fig 2. Ill-defined margins as a sign of malignancy. *A*, Warthin tumor with a well-defined border on axial T2-weighted imaging (*arrows*) in a 66-year-old man. *B*, Postcontrast T1-weighted imaging of Warthin tumor (*arrows*). *C*, Ill-defined margin (*arrows*) of a mucoepidermoid carcinoma in a 61-year-old male patient with SI similar to that in the Warthin tumor (*A*). Note the low SI on the T2-weighted image, which is also a malignant predictor. *D*, Postcontrast T1-weighted image of the ill-defined mucoepidermoid carcinoma (*arrows*).

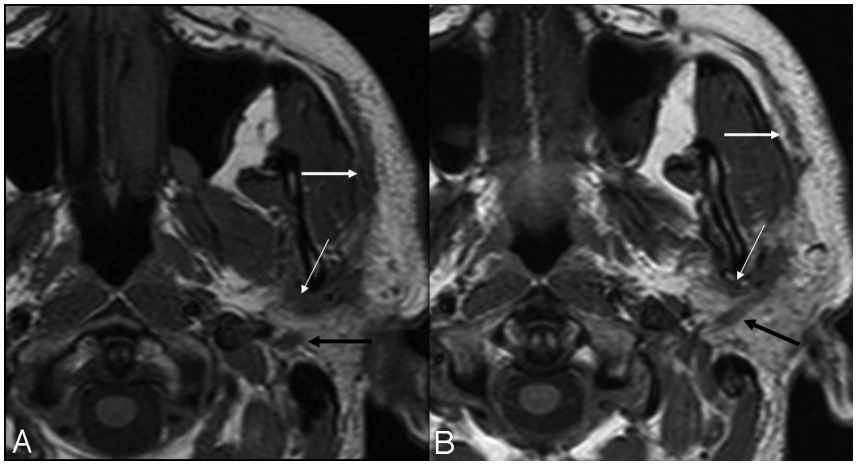

Fig 3. Undifferentiated carcinoma with perineural spread in a 43-year-old male patient. *A*, T1-weighted image shows perineural spread along the auriculotemporal (*thin white arrow*) branch of trigeminal nerve VIII, the facial nerve (*black arrow*), and the superficial branch of the facial nerve (*thick white arrow*). *B*, T1-weighted image of the same patient, a caudal view of image *A*. Note the longitudinal spread along the auriculotemporal (*thin white arrow*) and facial nerves: backward spread (*black arrow*) toward the stylomastoid foramen and forward spread along the superficial branch (*thick white arrow*).

Typical appearance of parotid tumors

Tumor	Appearance	*P* Value, Fisher Exact Test
Pleomorphic adenoma	Strong enhancement	.000026
	Defined boarders	.0018
	Polylobulated	.0024
	Superficial lobe	.0045
	Age, ≤57 yr[a]	.015[b]
	High SI T2-weighted ++	.022
Warthin tumor	Parotid tail	.0103
	Moderate SI TIRM +	.013
	Low enhancement	.015
Mucoepidermoid carcinoma	Low SI T2-weighted	.019
	Volume ≤1350 mm^{3a}	.037[b]
Adenoid cystic carcinoma	Low SI T2-weighted	.0499
Metastases	Subcutaneous infiltration	.0012
	Perineural spread	.0056
	Ill-defined margins	.0092
	Diffuse growth pattern	.011
	Multifocal	.014
	Located in both lobes	.016
	Moderate SI T2-weighted	.016

[a] Cutoff age and volume by ROC.
[b] Wilcoxon rank sum test.

tumor diagnosis (pathologic entity) between the benign and malignant group: Seventy percent of diagnoses of the benign cases and 37% of the malignant tumors were correct.

Typical MR imaging findings for the most frequently encountered parotid tumors in our cohort are listed in the Table.

Discussion

Among the well-known imaging findings that favor malignancy[1,2,3,10,13,19,21] from the current experience, "ill-defined margins postcontrast" was the single best discriminator with the lowest *P* value of .001.

Furthermore, our study confirms that T2 hypointensity of a parotid tumor is a useful indicator for malignancy ($P = .048$).[26] This finding has been previously linked to highly cellular tumors.[5,13,21] A simple malignancy test can be done by noting the presence of either T2 hypointensity or ill-defined margins postcontrast. The sensitivity and specificity of this simple MR imaging malignancy test are 0.70 and 0.73, respectively, which is very comparable with the original radiologic malignancy prediction (sensitivity of 0.67 and specificity of 0.81). Infection and inflammatory disease, particularly granulomatous inflammation, are very important differential diagnoses to consider because with inflammation, the edematous blurred lesional borders and diffuse involvement of the parotid gland mimic malignant tumor. Usually, inflammatory diseases display high SI on T2-weighted images, though chronic stages may have a somewhat lower SI.

The predilection of deep lobe involvement was only indicative but not significant for malignancy in our setting, because inflammatory disease and some benign tumors, like schwannoma and Warthin tumors, also affected the deep lobe. Because a schwannoma is located centrally along the facial nerve (VII), it may easily extend into both lobes. However, involvement of both lobes was significant for malignant lesions, like the superficial lobe affinity seen with benign tumors. Cystic/necrotic areas were not statistically significant for the diagnosis of malignant tumors because there was a high prevalence of cystic/necrotic regions in benign tumors like Warthin tumor or pleomorphic adenoma.

For determination of benign disease, a strong SI on T2-weighted images, well-defined borders, and a location in the superficial lobe were significant MR imaging findings for benignity. The degree of tumor enhancement after contrast administration did not help to distinguish benign from malignant tumors, though there was a tendency toward strong enhancement of benign tumors ($P = .16$).

The high SI on T2-weighted images of pleomorphic adenoma and their strong enhancement after contrast administration are well-known specific MR imaging findings, shown to be consistent with fibromyxoid stroma.[5-8] Furthermore, a polylobulated margin and younger patient age (<57 years) proved to be additional specific features for pleomorphic adenoma. From the previously described typical MR imaging findings of Warthin tumor,[2,3,9-12] our study confirmed the typical findings of heterogeneity of the tumor, moderate SI on TIRM images, absence of strong enhancement, and a location in the parotid tail. However, older age, bilaterality, and male predominance did not show a significant association with Warthin tumor. One explanation for the decreasing male predominance may be the growing number of female smokers, because smoking is one of the main risk factors for developing Warthin tumor.[27,28] As stated above, mucoepidermoid carcinoma has been previously described as a solid mass with cystic components (low-grade type) or an infiltrating lesion (high-grade type).[2,5,10] In our study, the single best MR imaging finding for mucoepidermoid carcinoma and also for adenoid cystic carcinoma was a low SI on T2-weighted images.

Sonography as a first line of investigation is particularly advantageous for assessing submandibular glands because they are superficial structures. The disadvantage of sonography is that it is operator-dependent, and assessment of deep structures, such as the deep lobe of the parotid gland and the relationship to the facial nerve, is suboptimal.[29,30]

The role of CT in assessing salivary gland tumors is limited. CT evaluates cortical mandibular involvement better and the presence of calculus disease in sialadenitis (which may mimic a tumor). MR imaging is superior in defining tumor characteristics and extension, particularly perineural spread.[29] It is especially useful when imaging is performed for suspected pleomorphic adenoma, because these lesions are typically hyperintense on the T2-weighted sequences and may be invisible on CT.[30] The drawbacks of MR imaging include the higher cost and longer examination time. Recently, new MR imaging techniques such as DWI and proton MR spectroscopy have shown promising results in the differentiation between benign and malignant salivary gland tumors.[31-35] However, the good DWI results for differentiating benign from malignant parotid gland lesions in 45 histologically proved tumors[32] could not be confirmed by the same group in a larger scale study evaluating 136 parotid tumors.[35] Although DWI was able to differentiate pleomorphic adenomas and myoepithelial adenomas from all other entities, a final differentiation between benign and malignant parotid gland tumors based on apparent diffusion coefficient values was not possible due to an overlap between the group of benign and malignant lesions and between groups.[35]

Limitations

We observed rare lesions, such as acinic cell carcinoma and granulomatous inflammation, which showed typical imaging appearances but which statistically could not be distinguished from other tumors. This result is likely related to the very small number of these lesions in our cohort, limiting statistical evaluation.

Because our study was designed for evaluation of the parotid gland and neck by using a standard neck MR imaging protocol, hematogenous spread of parotid tumors was not assessed, because the presence of hematogenous spread is rare and not an issue. Likewise, our standard protocol did not include dynamic contrast-enhancement and DWI sequences, which could add additional discriminatory information regarding tumor physiology. Nevertheless, as previously mentioned, recent studies also showed that DWI is not able to predict malignancy.[35] Future studies have to assess combined DWI and standard MR imaging.

Conclusions

Most benign and malignant parotid lesions can be discriminated by their appearance on MR imaging using a standard neck protocol before and after contrast medium administration. Low SI on T2-weighted images is a useful indicator for malignancy ($P = .048$). The presence of either T2 hypointensity or ill-defined margins after contrast administration can be a simple MR imaging malignancy test for parotid tumors, with a sensitivity and specificity of 0.70 and 0.73, respectively.

Acknowledgments

We are grateful to the team of highly motivated radiology technicians at our institution.

References

1. Batsakis JG. *Tumors of the Head and Neck*. 2nd ed. Baltimore: Williams and Wilkins; 1979:2–75
2. Freling NJ, Molenaar WM, Vermey A, et al. **Malignant parotid tumors: clinical use of MR imaging and histologic correlation.** *Radiology* 1992;185:691–96
3. Joe VQ, Westesson P. **Tumors of the parotid gland: MR imaging characteristics of various histologic types.** *AJR Am J Roentgenology* 1994;163:433–38
4. Swartz JD, Rothman MI, Marlowe FI, et al. **MR imaging of parotid mass lesions: attempts at histopathologic differentiation.** *J Comput Assist Tomogr* 1989;13:789–96
5. Rosai J Ackerman S. *Surgical Pathology.* 8th ed. St. Louis: Mosby; 1986:815–55
6. Tsushima Y, Matsumoto M, Endo K, et al. **Characteristic bright signal of parotid pleomorphic adenomas on T2-weighted MR images with pathological correlation.** *Clin Radiol* 1994;49:485–89
7. Ikeda K, Katoh T, Ha-Kawa SK, et al. **The usefulness of MR in establishing the diagnosis of parotid pleomorphic adenoma.** *AJNR Am J Neuroradiol* 1996;17:555–59
8. Mortele B, Lemmerling M, Seynaeve P, et al. **Hemangiopericytoma of the parotid gland: CT and MR features.** *Eur Radiol* 2001;11:1073–75
9. Motoori K, Yamamoto S, Ueda T, et al. **Inter- and intratumoral variability in magnetic resonance imaging of pleomorphic adenoma: an attempt to interpret the variable magnetic resonance findings.** *J Comput Assist Tomogr* 2004;28:233–46
10. Som PM, Curtin HD. *Head and Neck Imaging*. 3rd ed. St. Louis: Mosby; 1996:877–912
11. Lowe LH, Stokes LS, Johnson JE, et al. **Swelling at the angle of the mandible: imaging of the pediatric parotid gland and periparotid region.** *Radiographics* 2001;21:1211–27
12. Vogl TJ, Dtesel SH, Spath M, et al. **Parotid gland: plain and gadolinium-enhanced MR imaging.** *Radiology* 1990;177:667–74
13. Harnsberger HR. *Handbook of Head and Neck Imaging*. 2nd ed. St. Louis: Mosby; 1990:60–73
14. Sigal R, Monnet O, Baere T, et al. **Adenoid cystic carcinoma of the head and neck: evaluation with MR imaging and clinical-pathologic correlation in 27 patients.** *Radiology* 1992;184:95–101
15. Teresi LM, Lufkin RB, Wortham DG, et al. **Parotid masses: MR imaging.** *Radiology* 1987;163:405–09
16. Schlakman BN, Yousem DM. **MR of intraparotid masses.** *AJNR Am J Neuroradiol* 1993;14:1173–80
17. Mandelblatt SM, Braun IF, Davis PC, et al. **Parotid masses: MR imaging.** *Radiology* 1987;163:411–14
18. Minami M, Tanioa H, Oyama K, et al. **Warthin's tumor of the parotid gland: MR-pathologic correlation.** *AJNR Am J Neuroradiol* 1993;14:209–14
19. Takashima S, Wang J, Takayama F, et al. **Parotid masses: prediction of malignancy using magnetization transfer and MR imaging findings.** *AJR Am J Roentgenol* 2001;176:1577–84
20. Thoeny HC. **Imaging of salivary gland tumors.** *Cancer Imaging* 2007;7:52–62
21. Okahara M, Kiyosue H, Hori Y, et al. **Parotid tumors: MR imaging with pathological correlation.** *Eur Radiol* 2003(13 suppl 4):L25–33
22. Yabuuchi H, Fukuya T, Tajima T, et al. **Salivary gland tumors: diagnostic value of gadolinium-enhanced dynamic MR imaging with histopathologic correlation.** *Radiology* 2003;226:345–54
23. Takashima S, Noguchi Y, Okumura T, et al. **Dynamic MR imaging in the head and neck.** *Radiology* 1993;189:813–21
24. Tsushima Y, Matsumoto M, Endo K. **Parotid and parapharyngeal tumors: tissue characterization with dynamic magnetic resonance imaging.** *Br J Radiol* 1994;67:342–45
25. Divi V, Fatt MA, Teknos TN, et al. **Use of cross-sectional imaging in predicting surgical location of parotid neoplasms.** *J Comput Assist Tomogr* 2005;29:315–19
26. Yousem DM, Kraut MA, Chalian AA. **Major salivary gland imaging.** *Radiology* 2000;216:19–29
27. Sadetzki S, Oberman B, Mandelzweig L, et al. **Smoking and risk of parotid gland tumors: a nationwide case-control study.** *Cancer* 2008;112:1974–82
28. Freedman LS, Oberman B, Sadetzki S. **Using time-dependent covariate analysis to elucidate the relation of smoking history to Warthin's tumor risk.** *Am J Epidemiol* 2009;170:1178–85. Epub 2009 Sep 15
29. Lee YY, Wong KT, King AD, et al. **Imaging of salivary gland tumours.** *Eur J Radiol* 2008;66:419–36
30. Kei PL, Tan TY. **CT "invisible" lesion of the major salivary glands a diagnostic pitfall of contrast-enhanced CT.** *Clin Radiol* 2009;64:744–46
31. Wang J, Takashima S, Takayama F, et al. **Head and neck lesions: characterization with diffusion-weighted echo-planar MR imaging.** *Radiology* 2001;220:621–30
32. Habermann CR, Gossrau P, Graessner J, et al. **Diffusion-weighted echo-planar MRI: a valuable tool for differentiating primary parotid gland tumors?** *Rofo* 2005;177:940–45
33. King AD, Yeung DK, Ahuja AT, et al. **Salivary gland tumors at in vivo proton MR spectroscopy.** *Radiology* 2005;237:563–69
34. Thoeny HC, De Keyzer F, Boesch C, et al. **Diffusion-weighted imaging of the parotid gland: influence of the choice of b-values on the apparent diffusion coefficient value.** *J Magn Reson Imaging* 2004;20:786–90
35. Habermann CR, Arndt C, Graessner J, et al. **Diffusion-weighted echo-planar MR imaging of primary parotid gland tumors: is a prediction of different histologic subtypes possible?** *AJNR Am J Neuroradiol* 2009;30:591–96. Epub 2009 Jan 8